# All-fibre temperature sensor employing photonic crystal fibre-based Mach–Zehnder interferometer structure

GAOLIN QIN, QUANCAI LI, WEI WEI, JUNFA DUAN*
*School of Mechanical Engineering, North China University of Water Resources and Electric Power, Zhengzhou, 450045, China*

In this study, an all-fibre temperature sensor employing a photonic crystal fibre (PCF)-based Mach–Zehnder interferometer was manufactured by cascading single-mode fibre–multimode fibre (MMF)–PCF–MMF fusion splicing structure. For the sensor, the PCF length was 3 cm, and an interferometer comb spectrum free spectral range of 5.8 nm were realised. In the experiment, the temperature sensing characteristics during heating and cooling were measured; the sensitivity and linearity were 36 pm/°C within 30–60°C and >0.9715, respectively. Moreover, the sensor exhibited good stability and repeatability. The results demonstrate the satisfactory performance of the proposed sensor for temperature sensor applications.

(Received October 4, 2021; accepted April 7, 2022)

*Keywords:* Mach–Zehnder interferometer, Photonic crystal fibre, Single-mode fibre, Temperature sensing

## 1. Introduction

Fibre interferometer-type sensors have been widely used in applications, such as temperature, strain, stretch, refractive index, gas, displacement, and humidity measurements, because of their numerous advantages including compact structure, high sensitivity, anti-electromagnetic interference, corrosion robustness, and long work span [1-7]. Recently, some techniques for realising all-fibre temperature sensing applications have been reported. Liu et al. reported a temperature fibre sensor based on a Fabry–Perot (F-P) interferometer, comprising a single-mode fibre (SMF) and hollow-core fibre, with a sensitivity of 13.97 pm/°C [8]. Ma et al. described an S-taper fibre-based Mach–Zehnder interferometer (MZI) temperature sensor with a sensitivity of –15.66 nm/°C in the measurement range of 28–32 °C [9]. Chen et al. reported a dual-core fibre-based in-line MZI; the sensitivity of the proposed temperature sensor was –1.42 nm/°C [10]. Ma et al. reported a temperature fibre sensor based on a spiral-polished structure that was fabricated using a high-frequency $CO_2$ laser, wherein a sensitivity of 13.3 pm/°C was realised [11]. Ding et al. described a temperature sensor based on two cascaded high birefringence fibre loop mirrors, with a sensitivity of –23.68 nm/°C [12]. Yu et al. reported an all-fibre temperature sensor based on a side-hole fibre (SHF) structure, formed by SMF-coreless fibre (CLF)–SHF–CLF–SMF fusion splicing, with a sensitivity of 1.681 nm/°C in the range of 25–45 °C [13]. Lin et al. reported a cascaded fibre Sagnac loop-based ring fibre laser for temperature sensing, with a sensitivity of –4.031 nm/°C [14]. Wang et al. reported a temperature fibre sensor based on a tapered dispersion fibre with a temperature sensitivity of 79.8 pm/°C in the range of 25–60 °C [15]. Sakata et al. described a single – mode – multimode – single - mode structure interference temperature sensor, and a maximum sensitivity of 2 nm/°C was obtained in the temperature range of 40–70 °C [16].

As mentioned above, temperature fibre interferometer sensors have been manufactured using methods, such as the Sagnac loop, MZI, F-P, fibre loops, special fibres, and fragile optical microstructure components. The fibre interference fringes and their sensing capacity are determined by key filter components, and it is difficult to obtain an all-fibre temperature sensor with high sensitivity, repeatability, and mechanical strength. Unlike other methods, in our study, an all-fibre MZI incorporating a single-mode photonic crystal fibre (PCF) was designed and experimentally demonstrated.

## 2. Operation principle

The principle of the proposed fibre MZI sensor based on PCF is schematically shown in Fig. 1. The all-fibre sensor constitutes spliced SMF, multimode fibre (MMF), and PCF. The core/cladding diameters of the SMF and MMF are 9/125 and 105/125 μm, respectively, and the core/external cladding diameter of the PCF is 9/125 μm. Incident light is coupled into the MMF by the SMF, and high-order modes are generated. Then, the light is transmitted into the PCF, and separated into two beams at the PCF core and external parts, thus constructing an MZI. The two light beams converge at the second fusing point of the PCF and MMF, and the comb filter wavelength period can be expressed as shown in Eq. 1. Here, $\lambda$ is the transmission wavelength, $\Delta n_{eff}$ is the PCF effective refractive index of the core and external parts, and $\Delta L$ is the transmission length difference between the two beams. The wavelength period spacing $\Delta\lambda$ is inversely proportional to $L$.

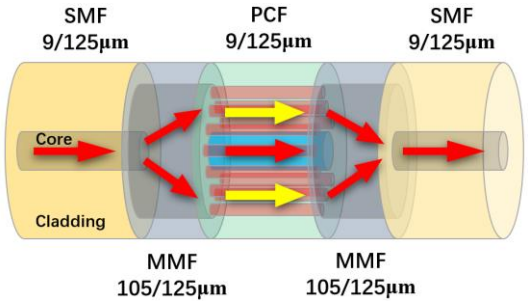


*Fig. 1. Schematic of the proposed PCF-based MZI (color online)*

$$\Delta\lambda = \frac{\lambda^2}{\Delta n_{eff}\Delta L} \tag{1}$$

When the temperature environment around the MZI is adjusted, the light paths of the core and external parts of the PCF change accordingly, and the MZI temperature sensitivity can be expressed using Equation 2. Here, $n_{external}$ is the effective refractive index of the PCF external part.

$$\frac{d\lambda}{dT} = \frac{[\frac{\lambda}{\Delta n_{eff}}(\frac{\partial \Delta n_{eff}}{\partial \Delta n_{core}}\cdot\frac{dn_{core}}{dT} + \frac{\partial \Delta n_{eff}}{\partial \Delta n_{external}}\cdot\frac{dn_{external}}{dT})] + \frac{\lambda}{\Delta L}\cdot\frac{d\Delta L}{dT}}{1-\frac{\lambda}{\Delta n_{eff}}\cdot\frac{\partial \Delta n_{eff}}{\partial \lambda}} \tag{2}$$

A schematic of the MZI temperature sensing system is shown in Fig. 2. The MZI fibre sensor was fixed on the temperature platform, a C+L broadband amplified spontaneous emission (ASE) light source was used, and an optical spectrum analyser (OSA; Yokogawa 6370) was adopted to collect the transmission spectrum. The circulator could be used in the system to eliminate reflected light of MZI.

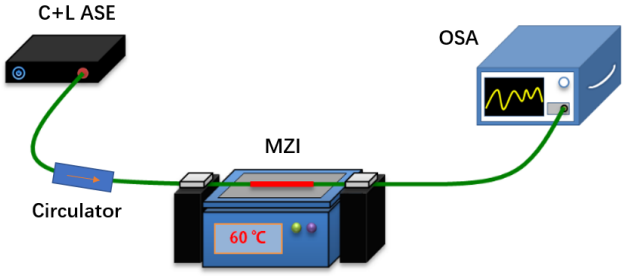


*Fig. 2. Schematic of MZI temperature sensing system (color online)*

## 3. Experimental results and discussion

In the experiment, the proposed fibre MZI was manufactured by fusing the SMF, MMF, and PCF. Because of the numerous air holes around the PCF core, the microchannel structure collapsed easily when the PCF and MMF were spliced, which was conducted according to the conventional method, as shown in Fig. 3(a). To solve these problems, the MMF was moved 30 μm beyond the fusion splitter electrodes, as shown in Fig. 3(b). Images of the MMF and PCF before and after splicing are shown in Figs. 3(c) and (d), respectively. After splicing the MMF and PCF successfully, the SMF and MMF were spliced to produce the SMF–MMF–PCF–MMF–SMF structure. For the proposed MZI comb filter, the reflection spectrum was measured, however, the intensity was not high, thus, the transmission spectrum was used for temperature sensing.

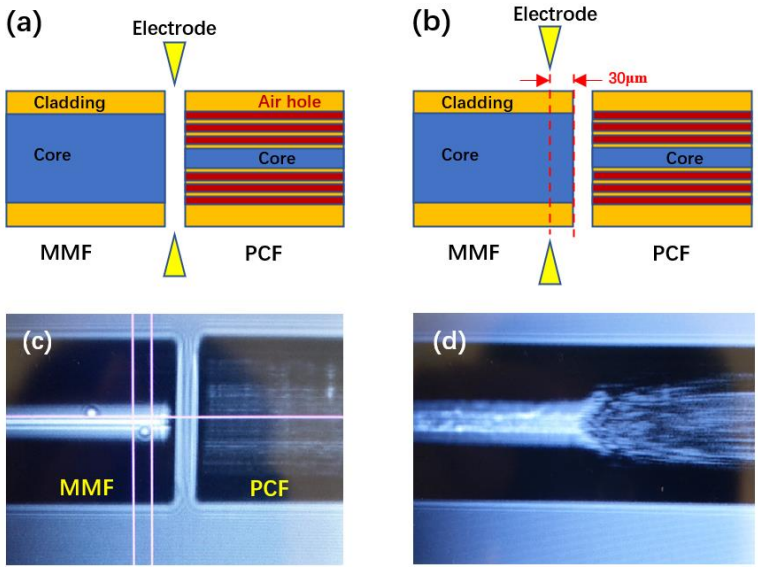


*Fig. 3. MMF and PCF splicing procedures. (a) Conventional method of splicing MMF and PCF. (b) Schematic of splicing MMF and PCF. Images (c) before and (d) after splicing (color online)*

The transmission spectrum of the proposed MZI was then measured, as shown in Fig. 4(a). When the length of the PCF was 2 cm, the comb interference effect was realised and the free spectral range was 18.2 nm. When the PCF length was 3 cm, the free spectral range was 5.8 nm, and the comb interference effect of the proposed fibre sensor was realized. As the PCF length increased, the interference period decreased. Additionally, the spectrum stability of the designed MZI at 30 °C was tested, as shown in Fig. 4(b); the wavelength fluctuation was not apparent during the 25-min monitoring time.

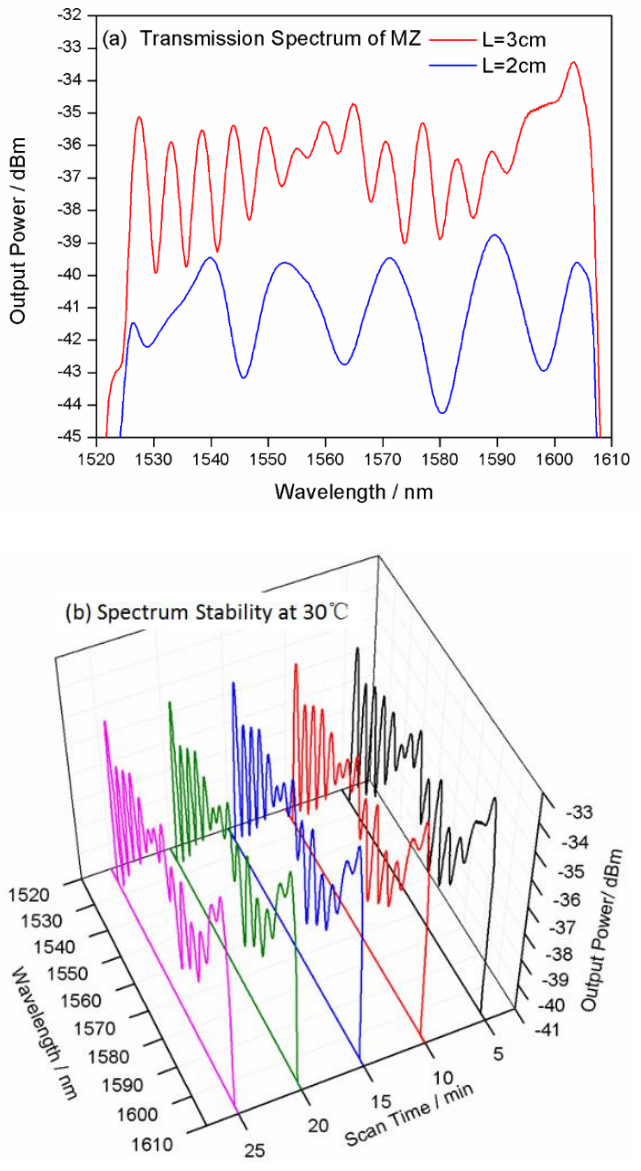


*Fig. 4. Spectrum characteristics of proposed MZI. (a) Transmission spectrum of MZI. (b) Spectrum stability of MZI at 30 °C (color online)*

In the experiment, the temperature sensing characteristics were tested. As shown in Fig. 5, the comb spectrum was tuned as the temperature was increased from 30 to 60 °C in increments of 5 °C, and the wavelength shifts are clear. The sensitivities of six sample points (dips a–f) in the C- (1,520–1,560 nm) and L-bands (1,560–1,600 nm) were analysed.

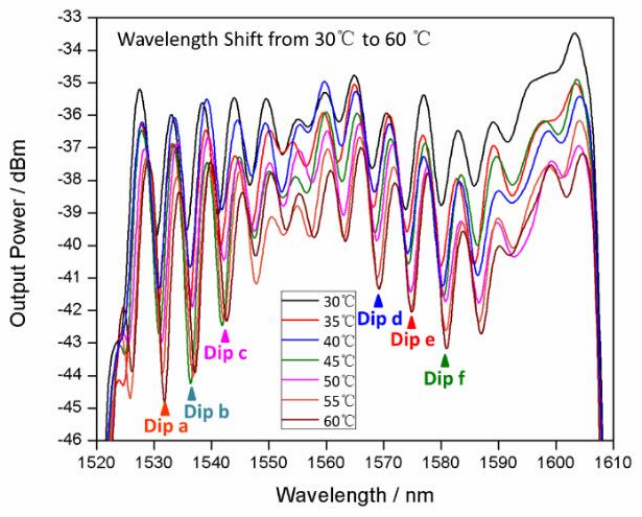


*Fig. 5. Spectrum characteristics for temperature sensing within C+L band (color online)*

As shown in Fig. 6(a), the wavelength shifts for dips a, b, and c moved toward the long-wavelength direction as the temperature increased. Meanwhile, the L-band sample points—dips d, e, and f—redshifted in the experiment, as shown in Fig. 6(b). The linear fitting curves of the six sample points were drawn, and the sensitivity values were calculated. As shown in Fig. 6(c), the sensitivities of dips a, b, and c are 41, 42, and 46 pm/°C, respectively, and the corresponding linearity values are 0.9715, 0.9894, and 0.978, respectively. For the L-band sample points—dips d, e, and f, the sensitivities are 42, 42, and 36 pm/°C, respectively, and the linearity values are 0.9948, 0.9894, and 0.9752, respectively. As shown in Fig. 6, the proposed MZI sensitivity remained greater than 36 pm/°C during the heating procedure.

The fibre sensing stability was tested at 60 °C. As shown in Fig. 7(a), evident wavelength shifts were not observed during the 25-min monitoring time. As shown in Fig. 7(b), the power fluctuations of dips b and d of the C- and L-bands were measured; the power variations of which were 0.12 and 0.08 dB, respectively. Thus, the proposed fibre sensor based on the MZI comb filter exhibits excellent stability.

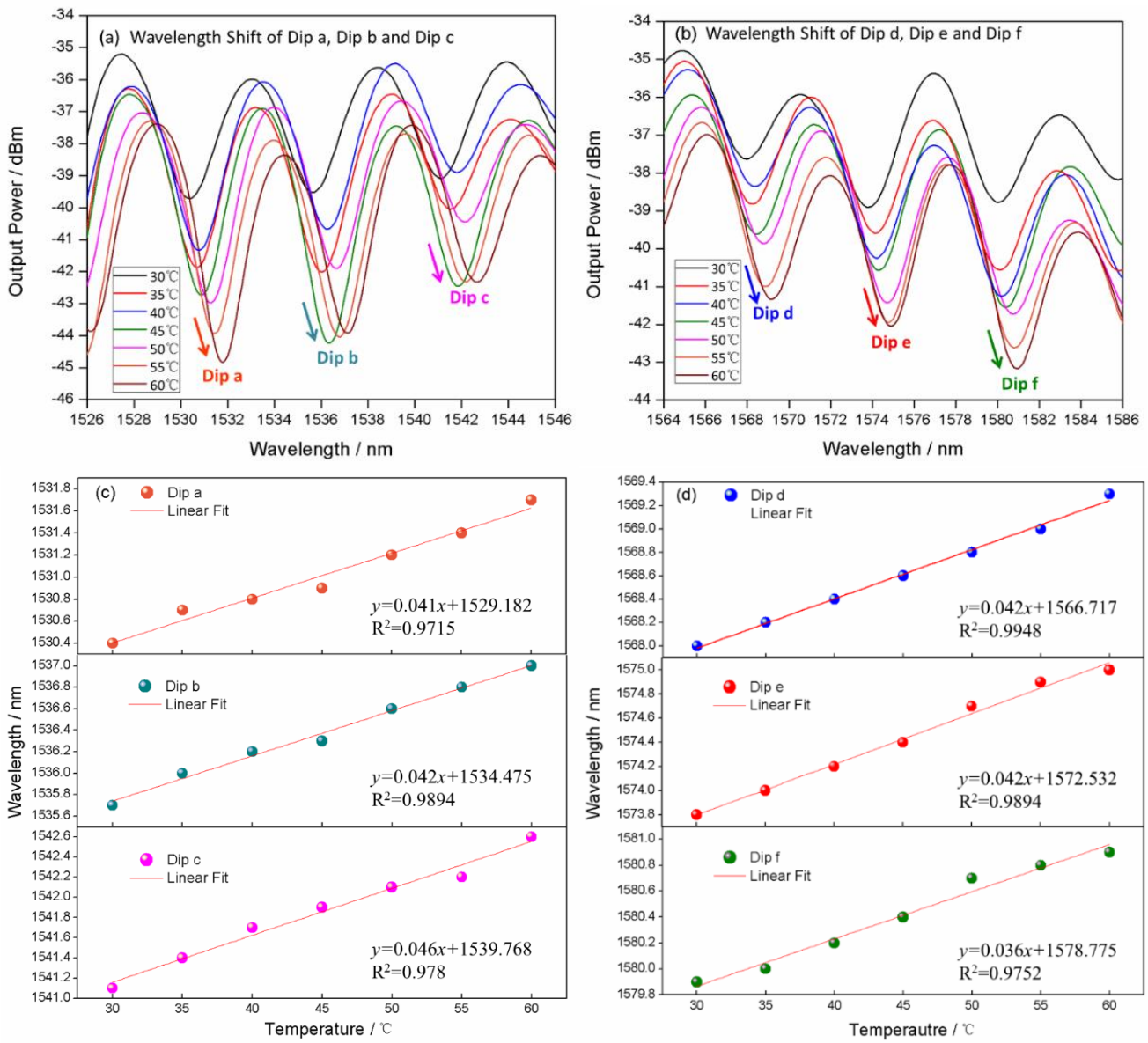


*Fig. 6. Temperature sensing characteristics of MZI during heating. Spectra of (a) dips a, b, and c; (b) dips d, e, and f. Sensitivities of (c) dips a, b, and c; (d) dips d, e, and f (color online)*

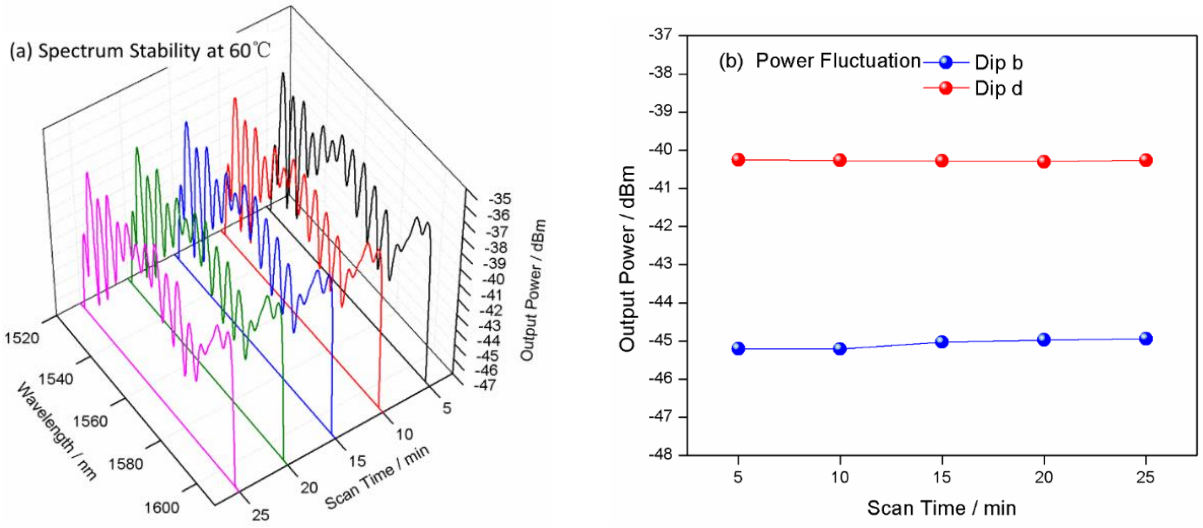


*Fig. 7. Stability of MZI at 60 °C. (a) Spectrum stability; (b) Power fluctuations of dips b and d (color online)*

In the experiment, the temperature sensing characteristics of the MZI during cooling were measured from 60 to 30 °C every 5 °C. As shown in Figs. 8(a) and (b), for sample points a–f, the spectrum shift moved toward the short-wavelength direction. The sensitivities of the C-band sample points are 43, 39, and 48 pm/°C, respectively, and the corresponding linearity values are 0.9751, 0.9822, and 0.9877, respectively, as shown in Fig. 8(c). For the three L-band sample points, the sensitivities were 44, 42, and 39 pm/°C, respectively, and the linearity values were 0.9825, 0.9949, and 0.9909, respectively. As shown in Fig. 8, the proposed MZI sensitivity was greater than 39 pm/°C during the cooling procedure.

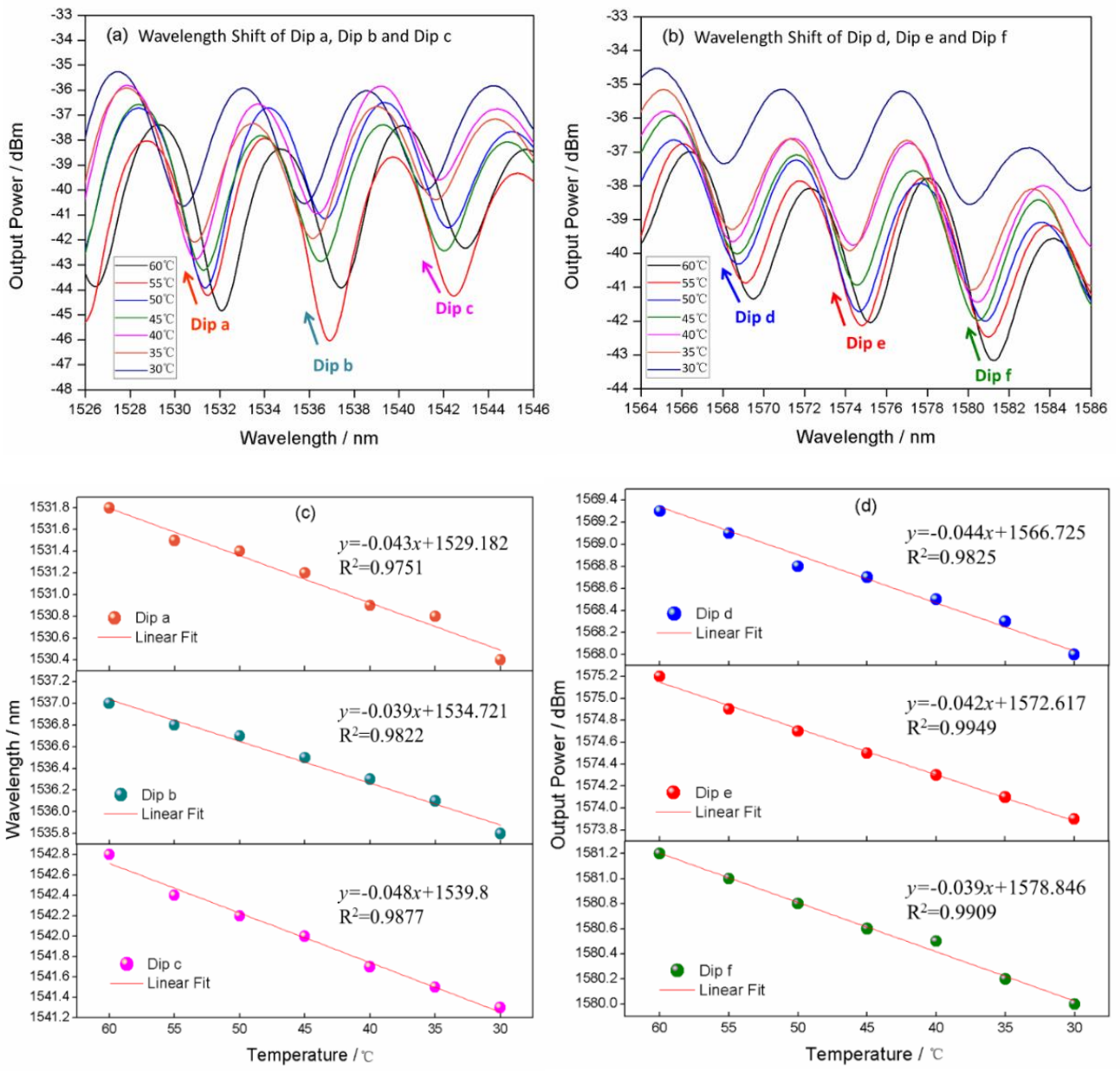


*Fig. 8. Temperature sensing characteristics of MZI during cooling. Spectra of (a) dips a, b, and c, and (b) dips d, e, and f; Sensitivities of (c) dips a, b, and c, and (d) dips d, e, and f (color online)*

The repeatability of the proposed MZI was analysed; dips b and d, respectively, were measured in the experiment during the heating and cooling procedures. As shown in Figs. 9(a) and (b), the proposed MZI exhibited excellent repeatability. The temperature sensitivity of MZI was related with heating platform, that was heat by resistance radiation, and temperature reduction was realized by nature cooling, the error was generated during heating and cooling procedure.

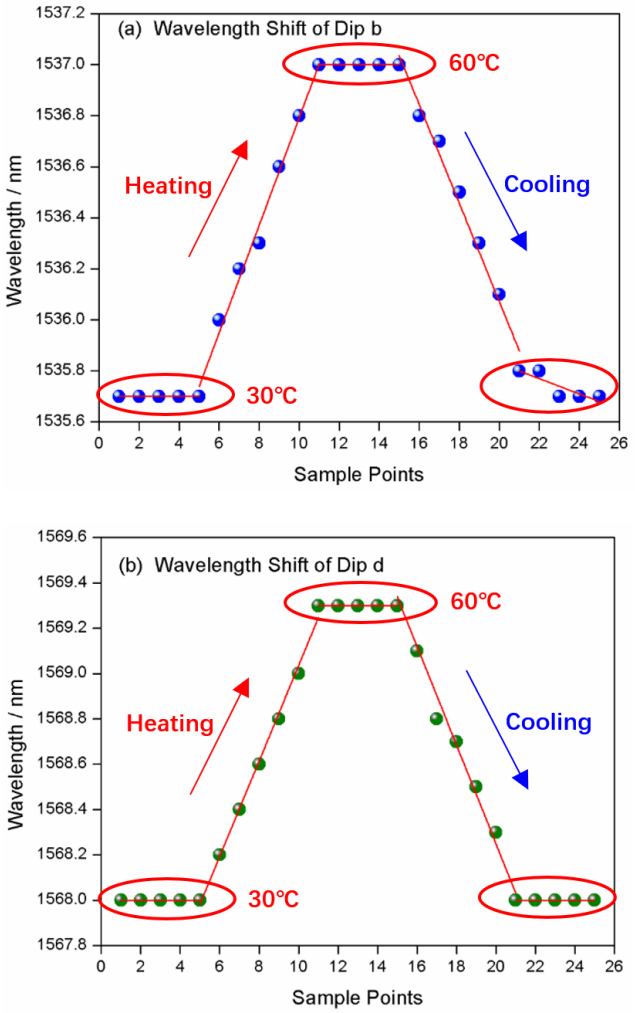


*Fig. 9. Repeatability of MZI temperature sensor. Wavelengths of (a) dips b and (b) d (color online)*

As demonstrated by the experiment described above, the proposed PCF-based MZI temperature sensor exhibits excellent sensitivity and stability.

## 4. Conclusions

In this study, an all-fibre MZI based on a PCF 3-cm length was realised. The proposed comb interferometer period was 5.8 nm. The temperature sensing characteristics of the heating procedure were measured; the sensitivity was more than 36 pm/°C in the range of 30–60 °C, and the linearity was more than 0.9715. For the temperature cooling procedure, the sensitivity and linearity were 39 pm/°C and 0.9825, respectively. Moreover, the proposed fibre sensor exhibited good stability and repeatability. The results demonstrate the satisfactory performance of the proposed sensor for temperature sensor applications. The proposed MZI sensor can be selected for multi-parameters measurement through cascaded with other fiber sensors, such as fiber grating, F-P, Sagnac loop and so on, because they have different sensitivity toward different measured object. Furthermore, it can be widely used in fibre sensing, spectral analysis, and comb filtering.

### Acknowledgements

This work was supported by the National Natural Science Foundation of China. [grant number: 51976012].

## References

[1] N. M. Azmi, N. H. Yusof, Z. Jusoh, H. A. Razak, S. W. Harun, Optoelectron. Adv. Mat. **12**, 272 (2018).
[2] S. Khanna, R. S. Kaler, Optoelectron. Adv. Mat. **10**, 151 (2016).
[3] H. Ahmad, S. N. Aidit, S. I. Ooi, Z. C. Tiu, IEEE Sens. J. **18**, 8275 (2018).
[4] H. L. Chen, Y. Zheng, B. C. Li, Y. D. Liu, Y. Y. Zhang, M. J. Ma, P. P. Shum, Opt. Laser Technol. **142**, 107193 (2021).
[5] H. C. Deng, X. W. Jiang, R. Wang, R. H. Xu, C. X. Teng, M. Chen, W. T. Zhang, L. B. Yuan, S. J. Deng, Opt. Commun. **496**, 127143 (2021).
[6] Z. C. Tiu, H. Haris, H. Ahmad, S. J. Tan, Microw. Opt. Techn. Let. **63**, 1314 (2020).
[7] Q. Tian, H. Z. Yang, K. S. Lim, Y. D. He, H. Ahmad, X. C. Liu, Optik **220**, 165034 (2020).
[8] H. Liu, H. Z. Yang, X. G. Qiao, M. L. Hu, Z. Y. Feng, R. H. Wang, Q. Z. Rong, D. S. Gunawardena, K. S. Lim, H. Ahmad, Sensor Actuat. A-Phys. **248**, 199 (2016).
[9] J. W. Ma, S. Wu, H. H. Cheng, X. M. Yang, S. Wang, P. X. Lu, Opt. Laser Technol. **139**, 106933 (2021).
[10] H. J. Chen, X. H. Hu, X. Y. Chen, Q. Q. Yu, Z. G. Lian, H. Wang, H. Qu, IEEE Sens. J. **21**, 12146 (2021).
[11] Y. W. Ma, C. B. Su, Y. Yi, M. Zhao, J. Sun, S. Y. Wang, X. Y. Li, G. Gao, S. N. Yu, C. G. Tong, W. M. Sun, L. B. Yuan, Appl. Phys. B-Lasers O **127**, 91 (2021).
[12] Z. C. Ding, Z. W. Tan, S. Y. Xiao, H. P. Gao, Appl. Phys. B-Lasers O **127**, 63 (2021).
[13] Z. Y. Yu, T. T. Lang, J. Hu, M. D. Chen, K. G. Ding, L. Y. Shao, Appl. Optics **60**, 3474 (2021).
[14] W. H. Lin, L. Y. Shao, Y. B. Liu, S. Bandyopadhyay, Y. H. Liu, W. J. Xu, S. Q. Liu, J. Hu, M. I. Vai, IEEE Photonics J. **13**, 3065567 (2021).
[15] F. Wang, L. Zhang, T. Ma, X. Wang, K. Yu, Y. F. Liu, Opt. Commun. **481**, 126534 (2021).
[16] H. Sakata, K. Okada, J. Mochizuki, Microw. Opt. Techn. Let. **63**, 1647 (2021).

*Corresponding author: duanjunfa@126.com